Homozygous deletion of glycogen synthase kinase 3β bypasses senescence allowing Ras transformation of primary murine fibroblasts

Shuying Liu*, Xianjun Fang[†], Hassan Hall*, Shuangxing Yu*, Debra Smith*, Zhimin Lu[‡], Dexing Fang[‡], Jinsong Liu[§], L. Clifton Stephens[¶], James R. Woodgett[‖], and Gordon B. Mills*,**

Departments of *Systems Biology, [§]Pathology, and [¶]Veterinary Medicine and Surgery, and [‡]Brain Tumor Center and Department of Neuro-Oncology University of Texas M. D. Anderson Cancer Center, Houston, TX 77030; [†]Department of Biochemistry and Molecular Biology, Virginia Commonwealth University, Richmond, VA 23284; and [‖]Samuel Lunenfeld Research Institute/Mount Sinai Hospital, Toronto, ON, Canada M5G 1X5

Edited by Tony Hunter, Salk Institute for Biological Studies, La Jolla, CA, and approved December 18, 2007 (received for review May 10, 2007)

In primary mammalian cells, expression of oncogenes such as activated *Ras* induces premature senescence rather than transformation. We show that homozygous deletion of glycogen synthase kinase (GSK) 3β (GSK3$\beta^{-/-}$) bypasses senescence induced by mutant Ras^{V12} allowing primary mouse embryo fibroblasts (MEFs) as well as immortalized MEFs to exhibit a transformed phenotype *in vitro* and *in vivo*. Both catalytic activity and Axin-binding of GSK3β are required to optimally suppress Ras transformation. The expression of Ras^{V12} in GSK3$\beta^{-/-}$, but not in GSK3$\beta^{+/+}$ MEFs results in translocation of β-catenin to the nucleus with concomitant up-regulation of cyclin D1. siRNA-mediated knockdown of β-catenin decreases both cyclin D1 expression and anchorage-independent growth of transformed cells indicating a causal role for β-catenin. Thus Ras^{V12} and the lack of GSK3β act in concert to activate the β-catenin pathway, which may underlie the bypass of senescence and tumorigenic transformation by Ras.

β-catenin | cyclin D1 | GSK3β

Immortalized rodent cells can readily be transformed by activated Ras or other oncogenes, leading to a transformed phenotype in culture and tumorigenicity *in vivo* (1, 2). However, in primary rodent cells activated Ras induces premature senescence (oncogene-induced senescence), decreasing oncogenesis (3–5). A second genetic alteration is required to bypass premature senescence and induce cellular transformation (6–9). A number of different genetic events bypass Ras-induced senescence including inactivation of the p53/p21/p19ARF pathway by aberrations in p53, p19ARF, PML, SIR2, DRIL1, TBX2, BCL6, or KLF4 (7–11), inactivation of Rb family proteins (3, 6, 7), activation of transforming growth factor (TGF)-β signaling (12, 13), and amplification of cellular or viral oncogenes including c-Myc and adenoviral E1A (14, 15). It is not clear whether these events represent a single pathway targeting the consequences of p53 signaling or whether there are multiple converging pathways or networks involved in the bypass of Ras-induced senescence. There are similarities between Ras-induced senescence and senescence of primary fibroblasts, particularly in the role of the p53/p21/p19ARF pathway (11). The p53 pathway induces plasminogen activator inhibitor-1 (PAI-1) with subsequent down-regulation of the phosphatidylinositol-3-kinase (PI3K)/Akt/PTEN/GSK3β-cyclin D1 pathway (16). Indeed, activation of the PI3K pathway with subsequent inactivation of GSK3β and up-regulation of cyclin D1 is sufficient to bypass p53-induced senescence and p53-induced senescence is associated with a decrease in signaling through the PI3K pathway (16).

The Wnt signaling pathway including Axin, APC and β-catenin is targeted by mutation in multiple tumor lineages (17). In mammalian cells, Wnt signaling is achieved, at least in part, by intracellular levels and localization of the oncoprotein β-catenin (18). The role of β-catenin in p53- and Ras-induced senescence may be complex as stabilized β-catenin induces p53-dependent senescence but cooperates with Ras to transform cells (19). In the absence of Wnt signals, a large multimeric protein complex that consists minimally of the scaffold protein Axin, APC, GSK3, and β-catenin is formed to sequester β-catenin to the cytosol and to regulate β-catenin levels (20–22). GSK3 phosphorylates β-catenin in the complex, targeting β-catenin for ubiquitination and subsequent degradation by a proteasome pathway (21, 22). Mutation or deletion of the putative GSK3 phosphorylation sites of β-catenin results in nuclear, constitutively active, highly stable forms of β-catenin, which are found in some colorectal cancers (23, 24). In addition to phosphorylation of β-catenin, GSK3β plays a linker role in the formation and recruitment of components of the Axin, APC, GSK3, and β-catenin complex (20–22). Although GSK3β has been proposed to integrate signals between the PI3K and β-catenin pathway, it is not clear whether the same or different pools of GSK3β mediate PI3K pathway signaling and regulate β-catenin function (25). GSK3$\beta^{-/-}$ MEFs have normal levels and localization of β-catenin (26), indicating that other kinases may act redundantly with GSK3β to control levels and localization of β-catenin.

We demonstrate that Ras^{V12} and lack of GSK3β act in concert to bypass senescence and transform primary mouse fibroblasts. The acquisition of the oncogenic phenotype is associated with activation of the β-catenin pathway, which may contribute the bypass of senescence and the tumorigenic transformation of primary cells.

Results and Discussion

Ras^{V12} Induces Premature Senescence in Wild-Type Primary MEFs but Not in MEFs Devoid of GSK3β. To investigate whether GSK3β contributes to oncogene-induced premature senescence, we isolated primary mouse fibroblasts from GSK3$\beta^{-/-}$ and GSK3$\beta^{+/+}$ embryos (26). Early passage (passage 3) primary MEFs were infected with pBabe-Ras^{V12} or control pBabe retrovirus. Puromycin-resistant cells were collected, and mutant Ras expression, loss of GSK3β and retention of GSK3α were confirmed by immunoblotting (Fig. 1*A*). Control virus-infected cells, either wild-type or GSK3β-negative, grew slowly showing little morphological difference from mock or uninfected cells. The majority of wild type MEFs infected with pBabe-Ras^{V12} (GSK3$\beta^{+/+}$/Ras) demonstrated a spreading and flattening morphology, typical of senescent cells. Senescence-associated acidic β-galactosidase (SA-gal) activity (27) was present in a large fraction of cells (Fig. 1*B*). In contrast, only a small fraction of GSK3$\beta^{-/-}$/Ras MEFs stained positive for SA-gal

Author contributions: S.L., X.F., and G.B.M. designed research; S.L., H.H., S.Y., D.S., D.F., and L.C.S. performed research; Z.L., J.L., and J.R.W. contributed new reagents/analytic tools; S.L. and G.B.M. analyzed data; and S.L., X.F., and G.B.M. wrote the paper.

The authors declare no conflict of interest.

This article is a PNAS Direct Submission.

**To whom correspondence should be addressed. E-mail: gmills@mdanderson.org.

This article contains supporting information online at www.pnas.org/cgi/content/full/0704242105/DC1.

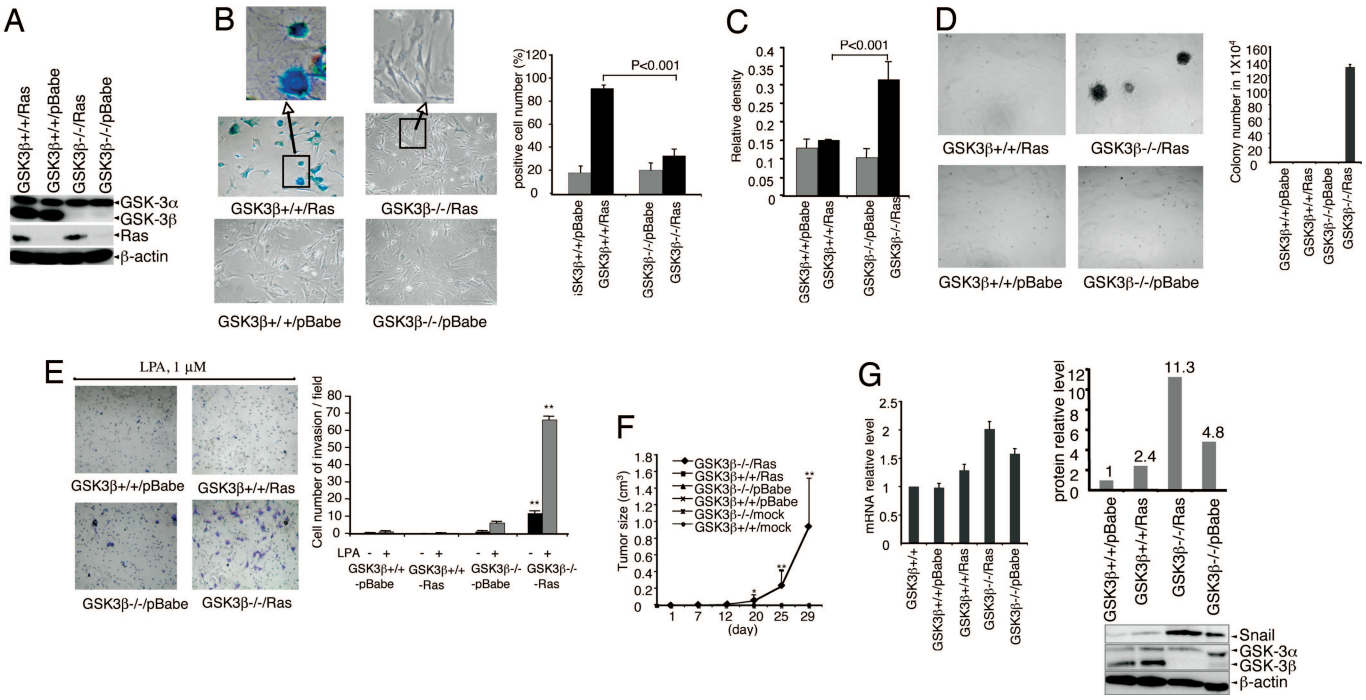

Fig. 1. Growth properties of Ras^{V12}- expressing primary MEFs. Primary MEFs were infected with control pBabe or pBabe-Ras^{V12} retrovirus. (*A*) Ras protein expression was verified by immunoblotting. (*B*) Primary MEFs (10th passage after infection with virus) were stained for SA-β-gal expression and the cells were photographed at ×100 magnification. The data are mean ± standard errors of triplicates, representative of two independent experiments. (*C*) Cell proliferation was assayed by crystal violet staining. Two independent experiments of triplicate assays were performed (*, $P < 0.001$). (*D*) A total of 4×10^4 primary MEFs infected with pBabe-Ras^{V12} or pBabe vector were plated on soft agar as detailed in *Methods*. Photomicrographs were taken 12 days after plating at × 40 magnification. The data are mean ± standard errors of triplicates, representative of two independent experiments (*$P < 0.0001$). (*E*) Ras-expressing GSK3$\beta^{-/-}$ MEFs invade through matrigel. The cells were photographed at ×100 magnification. The data are mean ± standard errors of triplicates, representative of two independent experiments ($P < 0.0001$). (*F*) A total of 4×10^6 primary MEFs infected with Ras^{V12} or vector retrovirus were injected s.c. into the right flank of nude mice. Photographs of the mice were taken at 29 days after cell injection. The data represents the average tumor size of four to seven mice from each group (*, $P < 0.05$; **, $P < 0.0001$). (*G*) (*Left*) Snail mRNA measured as fold change in MEFs. The data are the mean ± standard errors in two independent experiments. (*Right*) Relative Snail protein levels.

and occasionally demonstrated senescent morphology (Fig. 1*B*). GSK3$\beta^{+/+}$/Ras MEFs grew slowly in culture characteristic of loss of replicative capacity associated with senescence. In contrast, GSK3$\beta^{-/-}$/Ras MEFs continued to proliferate in complete medium containing 10% FBS and proliferated in response to lysophosphatidic acid (LPA) (Fig. 1*C*), one of the major growth factors present in serum (28–30). Thus, Ras-expressing GSK3$\beta^{-/-}$ MEFs bypass senescence and proliferate in culture.

Homozygous Deletion of GSK3β Allows Ras^{V12} to Transform Primary MEFs. We next examined whether GSK3$\beta^{-/-}$/Ras MEFs acquire a transformed phenotype. When GSK3$\beta^{-/-}$/Ras MEFs were plated in soft agar, they formed colonies (Fig. 1*D*), indicating that they acquired the ability to grow under anchorage-independent conditions. GSK3$\beta^{-/-}$ cells infected with control virus or wild type cells infected with either control or Ras^{V12} virus did not form colonies in soft agar. In addition, Ras^{V12}expression in GSK3$\beta^{-/-}$ MEFs, but not in wild type MEFs, conferred an invasive phenotype (Fig. 1*E*) in the presence or absence of LPA (28–30). Consistent with anchorage-independent growth and invasive phenotype *in vitro*, Ras^{V12}-expressing GSK3$\beta^{-/-}$ cells were highly tumorigenic in athymic nude mice, forming invasive tumors in 100% of injected mice (7/7) (Fig. 1*F*). In contrast, GSK3$\beta^{+/+}$/Ras MEFs were not tumorigenic. These results indicate that absence of GSK3β allows bypass of Ras-induced senescence facilitating transformation of primary MEFs. Thus, GSK3β functions to constrain transformation through contributing to oncogene-induced cellular senescence.

Snail, a critical regulator of epithelial mesenchymal transition, invasion and tumor growth, is regulated by GSK3β (31–33) potentially playing a role in invasiveness. Real-time quantitative PCR and immunoblotting showed that Snail RNA and protein levels are higher in GSK3β null than GSK3β wild type MEFs (Fig. 1*G*). Activated Ras cooperated with GSK3β loss to induce a marked increase in Snail levels (Fig. 1*G*) potentially contributing to increased invasion (Fig. 1*E*) and tumorigenesis (Fig. 1*F*) of Ras^{V12}-expressing GSK3$\beta^{-/-}$ cells.

GSK3α and GSK3β have been proposed to mediate redundant and overlapping functions (25, 34). However, Ras^{V12} did not transform GSK-3$\alpha^{-/-}$ primary MEFs (35) [supporting information (SI) Fig. 5], suggesting that GSK3α and GSK3β function differentially in cell senescence and transformation.

Homozygous Deletion of GSK3β Sensitizes Immortalized MEFs to Ras-Mediated Transformation. In contrast to primary cells, immortalized rodent cell lines are readily transformed by Ras^{V12} alone. To further explore the role of GSK3β in cell transformation, we took advantage of established GSK3$\beta^{-/-}$ and GSK3$\beta^{+/+}$ MEF lines (26). Early passages of the cells did not form colonies in soft agar or develop tumors in athymic nude mice (data not shown), indicating these MEF lines are immortalized but not transformed. Similarly, pooled puromycin-resistant colonies of GSK3$\beta^{-/-}$ and GSK3$\beta^{+/+}$ cells infected with the control virus did not form colonies in soft agar. Expression of Ras^{V12} in both GSK3$\beta^{-/-}$ and GSK3$\beta^{+/+}$ MEFs conferred an ability to grow under anchorage-independent conditions. However, Ras-expressing GSK3$\beta^{-/-}$ MEFs grew more profusely resulting in the formation of markedly

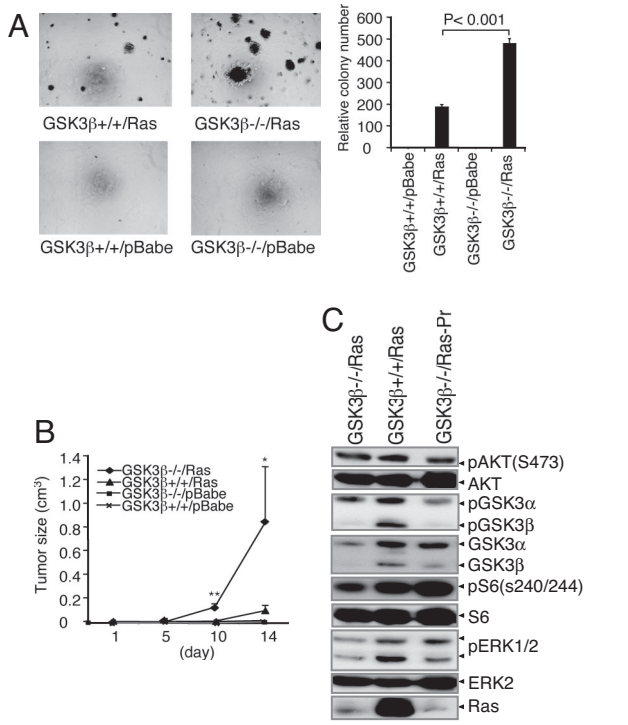

Fig. 2. Lack of GSK3β sensitizes Ras^{V12} transformation of immortalized MEFs. (*A*) Soft agar assay was performed as described in Fig. 1. (*B*) Comparison of tumorigenicity of Ras-expressing GSK3$\beta^{-/-}$ and GSK3$\beta^{+/+}$ MEF lines. A total of 2×10^6 MEFs were injected as xenografts into nude mice. The data represents the average tumor size of five mice of each group (*, $P < 0.05$; **, $P < 0.0001$). (*C*) Phosphorylation of Akt, GSK3α/β, ERK1/2, S6 ribosomal protein, and Ras protein expression were examined by immunoblotting in tumors derived from primary GSK3$\beta^{-/-}$ MEFs infected with Ras virus (GSK3$\beta^{-/-}$/Ras-Pr) or Ras expressing GSK3$\beta^{-/-}$ (GSK3$\beta^{-/-}$/Ras) or GSK3$\beta^{+/+}$ (GSK3$\beta^{+/+}$/Ras) immortal MEFs.

higher numbers and larger colonies in soft agar (Fig. 2*A*). Consistent with the results of anchorage-independent growth, Ras^{V12}-expressing GSK3$\beta^{-/-}$ MEFs formed more rapidly growing tumors in nude mice than Ras^{V12}-expressing GSK3$\beta^{+/+}$ cells (Fig. 2*B*). Most of the tumors derived from Ras^{V12}-expressing GSK3$\beta^{-/-}$ cells reached a size of 1 cm^3 within 2 weeks of injection, whereas Ras^{V12}-expressing GSK3$\beta^{+/+}$ cell-derived tumors remained <0.2 cm^3. Control virus transduced GSK3$\beta^{-/-}$ or GSK3$\beta^{+/+}$ cells did not form palpable tumors (0/5).

Inactivation of the p53/p21/p19ARF pathway can bypass senescence induced by Ras and cooperate with Ras to transform cells (7–11). However, as both GSK3$\beta^{-/-}$ and GSK3$\beta^{+/+}$ immortalized MEFs have lost p53, the cooperative interaction between activated Ras and loss of GSK3$\beta^{+/+}$ is independent of effects on the p53 pathway.

Activation of the PI3K pathway has been suggested to be sufficient to bypass p53-induced senescence (16). However, as demonstrated by Western blot analysis (Fig. 2*C*), phosphorylation levels of Akt, Erk and S6 Ribosomal Protein in tumors derived from Ras^{V12}-expressing immortal GSK3$\beta^{-/-}$ cells (GSK3$\beta^{-/-}$/Ras) and primary cells (GSK3$\beta^{-/-}$/Ras-Pr) were not higher than in tumors derived from Ras^{V12}-expressing GSK3$\beta^{+/+}$ cells (the low levels of GSK3β in the GSK3$\beta^{-/-}$ tumors likely reflects the presence of host stroma cells). In addition, Ras expression levels in the tumors derived from Ras^{V12}-expressing GSK3$\beta^{+/+}$ were much higher than those in the tumors derived from Ras^{V12}-expressing GSK3β null cells (Fig. 2*C*), suggesting that, although Ras can transform immortalized wild type MEFs, higher levels of Ras are required.

Reexpression of GSK3β Suppresses Ras-Induced Transformation. The enhanced susceptibility of GSK3β null MEFs to Ras-induced oncogenic transformation could potentially be due to clonal variation in the two immortal MEF lines rather than the lack of GSK3β. To evaluate this possibility, we reexpressed GSK3β in the GSK3$\beta^{-/-}$ MEF line by infection with a GSK3β retrovirus that coexpresses GFP (36). Highly enriched populations of >90% GFP-positive cells were sorted and isolated by flow cytometry. The expression of GSK3β was confirmed by Western blotting (data not shown). Similar to the wild-type MEF line, the reexpressing GSK3β cells were less susceptible to transformation induced by the pBabe-Ras^{V12} retrovirus compared with the control GSK3$\beta^{-/-}$ cells as reflected by decreased anchorage-independent growth and tumorigenicity in nude mice (Fig. 3 *A* and *B*). This observation confirms the role of GSK3β in inhibition of Ras-induced transformation in immortalized MEFs.

GSK3β Suppresses Ras Transformation Through both Catalytic and Axin-Binding Activity. GSK3β functions both as a kinase regulating β-catenin phosphorylation and as a structural component of the APC/Axin/GSK3β/β-catenin complex (25, 37). We thus examined whether the kinase activity of GSK3β is required to suppress Ras-induced cell transformation. To this end, we assessed a kinase-

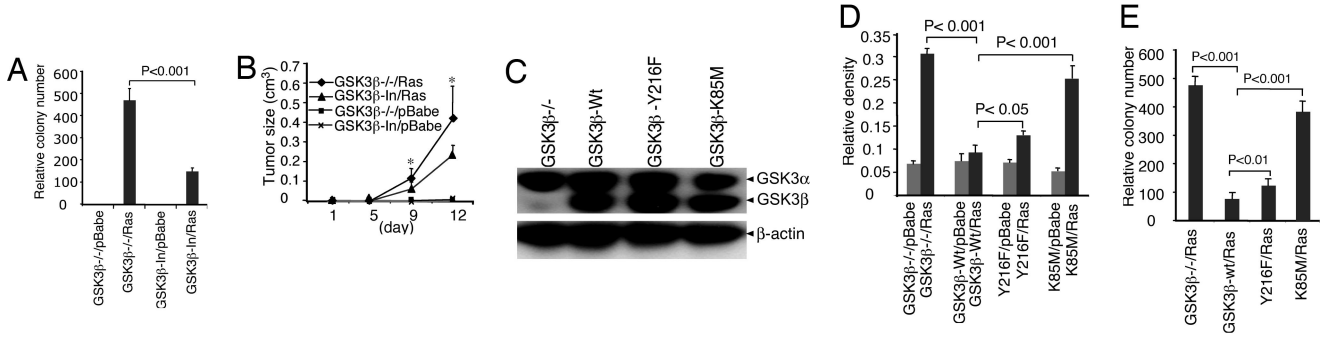

Fig. 3. GSK3β reexpression suppresses Ras-induced cell transformation in GSK3β both kinase and Axin-binding activity-dependent manner. Immortalized GSK3$\beta^{-/-}$ MEFs were infected with wild type GSK3β (GSK3β-In) or control retrovirus. GFP-positive cells were sorted and infected with Ras virus or control pBabe virus. (*A*) Soft agar assay was performed as described in Fig. 1& Fig. 2. (*B*) Tumorigenicity assays in nude mice as described in Fig. 2. Each data point of growth curves represents the average tumor size of 5 mice in each group. Tumors that did not grow were assigned a volume of zero (* $P < 0.05$). (*C*) GSK3$\beta^{-/-}$ MEFs were infected with retrovirus carrying mutant GSK3β (GSK3β-K85M, GSK3β -Y216F) in comparison with that carrying wild type GSK3β (GSK3β-Wt). GSK3 protein expression was verified by immunoblotting. The GSK3β null and GSK3β (wild type or mutants) reexpressing immortal MEFs were infected with Ras virus or control pBabe virus. Transduced cells were analyzed for growth in culture by crystal violet colorimetric staining (*D*) and by soft agar assays (*E*), as detailed in *Methods* and Fig. 1.

dead mutant of GSK3β (K85M) which also lacks the ability to bind to the scaffold protein Axin and a hypomorphic mutant (Y216F) with markedly decreased kinase activity that has been reported to retain Axin binding (36, 38, 39). Highly enriched GFP-positive cells were isolated by flow cytometry and expression of GSK3β confirmed by Western blotting (Fig. 3*C*). In contrast to wild-type GSK3β, the K85M mutant, which lacks kinase activity and Axin binding, did not inhibit anchorage-dependent (Fig. 3*D*) or -independent growth (Fig. 3*E*) of Ras-expressing GSK3$\beta^{-/-}$ cells, suggesting the importance of GSK3β kinase activity and/or Axin binding in inhibition of Ras transformation. In contrast, expression of the hypomorphic mutant (Y216F) of GSK3β led to marked inhibition of anchorage-dependent and -independent growth of Ras-expressing GSK3$\beta^{-/-}$ cells compared with GSK3$\beta^{-/-}$ or K85M mutant cells; however, the Y216F mutant was less effective than wild type (Fig. 3 *D* and *E*). Thus, both kinase and Axin-binding activity appear required for GSK3β to optimally suppress Ras transformation.

Ras^{V12} and the Lack of GSK3β Act Coordinately to Induce Nuclear Localization of β-Catenin Increasing Cyclin D1 Expression in Primary MEFs. The interactions between GSK3β and β-catenin, a key regulator of cell growth, motility and transformation, prompted us to determine whether Ras and knockout of GSK3β could act in concert to induce β-catenin nuclear translocation, leading to activation of the β-catenin pathway (26, 40, 41). Neither homozygous disruption of GSK3β nor Ras^{V12} expression in wild type primary MEFs was sufficient to induce nuclear β-catenin accumulation (Fig. 4*A*). However, Ras-expressing primary GSK3$\beta^{-/-}$ MEFs exhibited striking increases in nuclear β-catenin (Fig. 4*A Upper*), indicating that coordinate expression of Ras^{V12} and deletion of GSK3β promotes nuclear translocation of β-catenin. Consistent with the localization of β-catenin to the nuclei of GSK3$\beta^{-/-}$ Ras cells in culture, significant staining of nuclear β-catenin was observed in the nuclei of GSK3$\beta^{-/-}$ Ras tumor cells *in vivo*, suggesting that the change in β-catenin localization persists *in vivo* (Fig. 4*A Lower*).

Because lack of GSK3β alone was not sufficient to induce the nuclear accumulation of β-catenin, GSK3α may play a key role in inducing β-catenin degradation in GSK3β null MEFs. To assess this possibility, we examined phosphorylation of β-catenin at Ser-33 and -37 and Thr-41, through which GSK3 destabilizes β-catenin (42). As shown in Fig. 4*B*, these sites were indeed phosphorylated in GSK3β-negative MEFs likely by GSK3α and phosphorylation levels were decreased upon introduction of Ras. The inhibition of β-catenin phosphorylation at Ser-33 and -37 and Thr-41 by oncogenic Ras in GSK3$\beta^{-/-}$/Ras cells is apparently not mediated by the Ras-P13K-Akt pathway as phosphorylation of GSK3α at Ser-21 by Akt was not increased in GSK3$\beta^{-/-}$/Ras cells. In addition, phosphorylation of β-catenin by casein kinases CK1 at Ser-45, a priming site for the subsequent phosphorylation by GSK3, was also inhibited by introduction of Ras^{V12} in GSK3β null cells but not in wild-type cells (Fig. 4*B Upper*).

Activation of dishevelled (Dvl) promotes Wnt/β-catenin signaling (43–45). We thus examined phosphorylation of dishevelled-3 (Dvl-3) as a readout for the effect of Ras^{V12} on activation of the Wnt pathway in the presence and absence of GSK3β. Phosphorylation of Dvl-3 as indicated by a size shift on Western blotting (46) was increased in GSK3$\beta^{-/-}$/Ras cells compared with GSK3$\beta^{-/-}$ or Ras^{V12}-expressing GSK3$\beta^{+/+}$ cells suggesting that Ras^{V12} enhances Wnt signaling in GSK3$\beta^{-/-}$ cells (Fig. 4*B Upper*). Consistent with the enhanced Wnt signaling, we also observed an increase in Wnt-3 expression and a concurrent decrease in sFRP-2 levels in GSK3$\beta^{-/-}$/Ras^{V12} cells as compared with GSK3$\beta^{-/-}$ cells (Fig. 4*B Lower*). These results together indicate that multiple mechanisms are involved in activation of β-catenin in GSK3$\beta^{-/-}$/Ras cells.

Cyclin D1 is a downstream target of both the β-catenin-TCF transcription factor and GSK3 (47–49). Furthermore, cyclin D1 levels and localization are altered in senescent cells and expression of a stable nuclear cyclin D1 can bypass p53-induced senescence (16). Serum induced a more robust accumulation of cyclin D1 in GSK3$\beta^{-/-}$/Ras MEFs than in GSK3$\beta^{+/+}$/Ras MEFs (Fig. 4*C*). Expression of c-Jun, but not c-Myc, was also enhanced in GSK3$\beta^{-/-}$/Ras MEFs (SI Fig. 6). Thus, the nuclear translocation of β-catenin induces target gene expression. To determine whether β-catenin was required for the increased induction of cyclin D1 in GSK3$\beta^{-/-}$/Ras MEFs, β-catenin expression was down-regulated with siRNA and shRNA. As determined by immunoblotting and immunofluorescence staining, transfection with β-catenin RNAi reduced β-catenin by 70–80% (Fig. 4*D*) in GSK3$\beta^{-/-}$/Ras MEFs with a concomitant decrease in cyclin D1 induction, an effect not observed with nontargeted RNAi (Fig. 4*E*). Silencing β-catenin with siRNA or shRNA also decreased anchorage-independent growth of GSK3$\beta^{-/-}$/Ras MEFs (Fig. 4*F*), indicating that the β-catenin pathway contributes to the transformation of primary MEFs induced by coordinate expression of activated Ras and loss of GSK3β.

In summary, we have demonstrated that GSK3β-negative primary MEFs bypass Ras^{V12} induced senescence acquiring a transformed phenotype. Our results reveal that Ras mutation and the absence of GSK3β act in concert to transform primary murine fibroblasts. The cooperative effects of Ras^{V12} and lack of GSK3β on the β-catenin-cyclin D1 pathway provide a potential mechanism for the observed synergism between Ras and lack of GSK3β in the bypass of senescence and transformation of primary cells. These studies establish a role for GSK3β in oncogene-induced senescence of primary cells limiting oncogene-induced transformation.

Methods

Cells. MEF cell lines isolated from GSK3$\beta^{-/-}$ mouse embryo and wild-type littermate were established in culture as immortal lines as described previously (26). The immortal MEF lines lack p53 expression (not presented). MEFs were cultured in high-glucose DMEM supplemented with 10% FBS, 100 units/ml penicillin and 100 μg/ml streptomycin. Cells were frozen at early passages and used for less than 4 weeks in continuous culture. Primary MEFs from GSK3$\beta^{+/+}$ and GSK3$\beta^{-/-}$ mouse embryos were cultured in the same medium supplemented with 1 mM sodium pyruvate.

Retrovirus Constructs (LZRS-EGFP-GSK3β, LZRS-EGFP-GSK3β-K85M, LZRS-EGFP-GSK3β-Y216F, pBabe, and pBabe-Ras^{V12}). Retroviral constructs for HA-GSK3β, HA-GSK3β-K85M, and HA-GSK3β-Y216F were described in ref. 36. The pBabe vector and pBabe-Ras^{V12} were from S. Lowe (Cold Spring Harbor Laboratory, Cold Spring Harbor, NY).

Generation of Retrovirus. The retrovirus constructs (LZRS-EGFP, LZRS-EGFP-GSK3β, LZRS-EGFP-GSK3β-K85M or LZRS-EGFP-GSK3β-Y216F, pBabe, and pBabe-Ras^{V12}) were transfected into the BOSC23 packaging line using Lipofectamine 2000 as described elsewhere (36). After infection with pBabe or pBabe-Ras^{V12}, transduced cells (colonies) were selected by culture with puromycin (for immortal cells, 2 μg/ml for 2 weeks; for primary cells, 1 μg/ml for 3 days).

Western Blotting and Antibodies. Western blot analysis was performed as described (36). Pan-Ras Val^{12} (Calbiochem), β-actin (Sigma), GSK3, Wnt-3, sFRP-2, sFRP-3 (Santa Cruz Biotechnology), β-catenin, cyclin D1, pAkt (Ser-473), pS6 (S240/244), pERK1/2, pGSK3α/β (S21/9), p-β-catenin (S45), p-β-catenin (Ser-33/37/Thr-41), β-catenin, Dvl-3 (Cell Signaling) and Snail (Abcam) antibodies were used for immunoblotting.

RNA Isolation and Real-Time Quantitative PCR. Total cellular RNA was isolated from MEFs with TRIzol according to the manufacturer's protocol (Invitrogen). Fluorogenic Taqman probes, Taqman One-Step RT-PCR master reagent and Taqman GAPDH detection kit were from Applied BioSystems. Snail mRNA level was determined by Taqman real-time RT-PCR using the ABI PRISM 7700 Sequence Detection System (Applied Biosystems) through 40 cycles, with GAPDH as a reference.

SA-β-Galactosidase Staining. Staining for SA-β-gal activity in cultured cells was carried out using a staining kit (Chemicon International Inc/Specialty Media). Briefly, cells were seeded and cultured in 30-mm dishes. After washing with PBS,

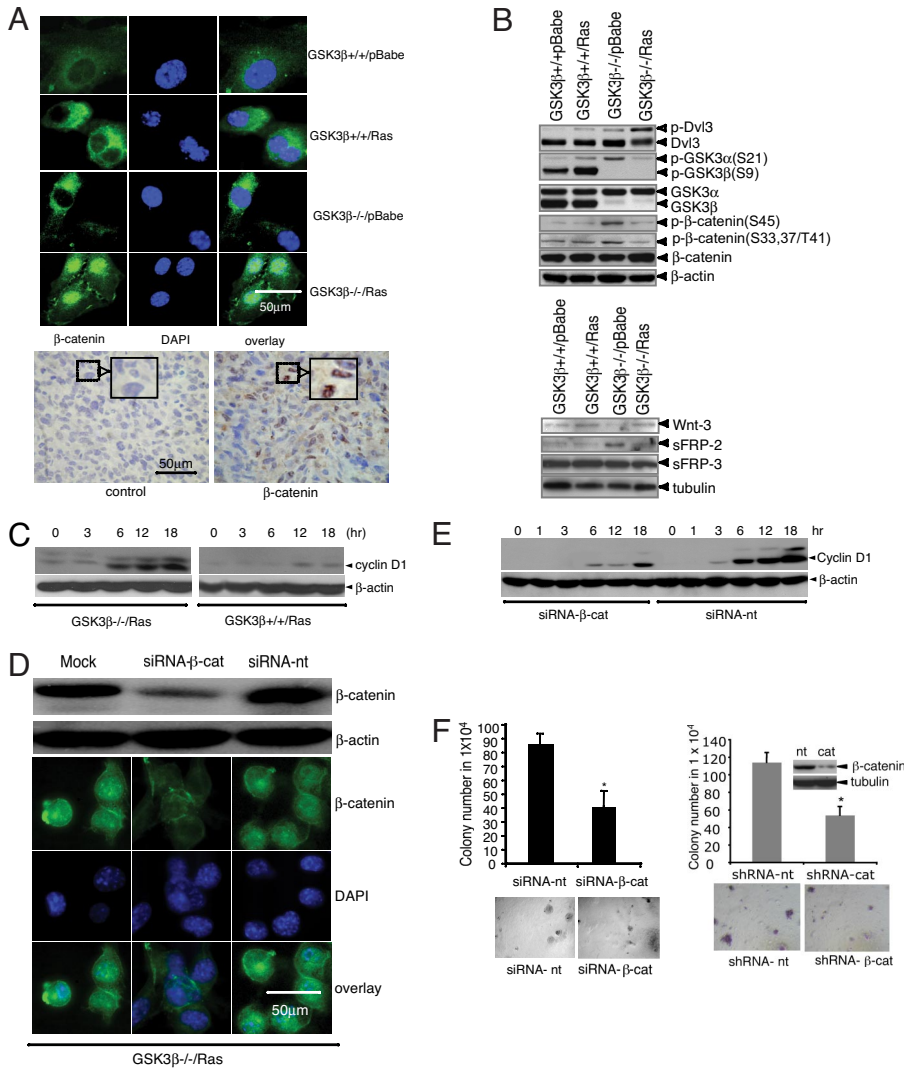

Fig. 4. Ras^{V12} and lack of GSK3β act in concert to activate the β-catenin pathway. (*A*) Ras expressing primary MEFs were starved in serum-free DMEM for 24 h, and then cultured in complete growth medium overnight. Cells were fixed and immunostained with antibodies to β-catenin (20.0 μg/ml; Biosource, CA) to determine the contents and localization of β-catenin. Nuclei were stained with DAPI (*Upper*). Immunohistochemical staining of β-catenin in the xenografts derived from Ras transformed GSK3$\beta^{-/-}$ MEFs. Paraffin-embedded sections were stained with or without (control) primary anti-β-catenin antibody (*Bottom*). (*B*) Phosphorylation of GSK3α/β, β-catenin (Ser-33/37/Thr-41), β-catenin (Ser 45) and Dvl-3 (*Top*) and Wnt-3, sFRP-2 and sFRP-3 (*Lower*) were examined by immunoblotting in Ras expressing primary MEFs. (*C*) Ras^{V12}-expressing primary GSK3$\beta^{-/-}$ and GSK3$\beta^{+/+}$ MEFs were starved in serum-free DMEM for 24 h and cultured in complete growth medium as indicated. Expression of cyclin D1 was analyzed by immunoblotting. Reprobing for β-actin was included as loading control. (*D*) GSK3$\beta^{-/-}$/Ras MEFs were transfected with either mouse-specific β-catenin (siRNA-β-cat) or nontargeting siRNA (siRNA-nt) using Lipofectamine 2000. Forty-eight hours after transfection, β-catenin expression was analyzed by immunostaining or Western blotting. Reprobing for β-actin was included as loading control. (*E*) GSK3$\beta^{-/-}$/Ras MEFs were transfected with β-catenin siRNA. 36 h later, the cells were cultured in serum free DMEM for overnight. The cells were then incubated in complete growth medium for the indicated hours and analyzed by immunoblotting for cyclin D1 and β-actin (loading control). (*F*) The anchorage-independent growth of the cells after siRNA (*Left*) or shRNA (*Right*) knockdown of β-catenin expression was assessed in soft agar assay as described in Fig. 1. The data are mean $\pm$ standard errors of triplicates in two independent experiments ($P < 0.001$).

the cells were fixed with β-Gal Fixative and stained with Complete β-Gal Stain Solution followed by addition of β-Gal Holding Solution.

Cell Proliferation Assay. Cell numbers were assessed by staining with crystal violet as an indicator of DNA content. Cells were seeded in 96-well plates (5×10^3 per well) in complete DMEM. After overnight starvation, the cells were stimulated with LPA (5 μM) or vehicle (0.5% BSA in PBS) for 48 h and stained with 0.5% crystal violet in 20% methanol for 20 min. Sorenson's Buffer [0.1 mol/liter sodium citrate (pH 4.2) and 50% ethanol] was added to each well and incubated for 2 h. Absorbance was measured at 570 nm with a microplate autoreader.

***In Vitro* Invasion Assay.** Invasion was analyzed with 24-well Biocoat Matrigel invasion chambers with 8-μm polycarbonated filters (Becton Dickinson). Cells were starved for 20 h in serum-free DMEM. After washing with serum-free DMEM, 1×10^4 cells in 0.5 ml DMEM were inoculated into the upper chamber and 0.75 ml DMEM containing LPA (1 μM) or vehicle (0.5% BSA in PBS) was added to the lower chamber. The cells were allowed to migrate through the Matrigel at 37°C, 5% CO_2 for 24 h. Nonmigrated cells on the upper surface of the filter were removed by wiping with a cotton swab. The cells that penetrated through pores of the Matrigel to the underside of the filter were stained with 0.25% crystal violet in 20% methanol for 30 min. Migrated cells were photographed and counted in 10 random fields.

Soft-Agar Assay. Cells were suspended in complete DMEM containing 0.3% soft agar and seeded in triplicate on 60-mm dishes precoated with 0.6% agar in complete growth medium and incubated at 37°C, 5% CO_2. After 12–14 days, colonies were photographed and counted in 10 randomly chosen fields and expressed as means of triplicates, representative of two independent experiments.

Tumor Xenografts in Athymic *nu/nu* Mice. Female athymic (*nu/nu*) mice were purchased from the National Cancer Institute (Frederick, MD) at 6 weeks of age and were housed in appropriate sterile filter-capped cages. All animal studies were carried out under ACUF-approved protocols. Exponentially growing cells were harvested, washed, and resuspended in 200 μl PBS, and 2×10^6 (immortalized) or 4×10^6 (primary) cells were injected s.c. into the right flank of athymic mice. Tumor sizes were determined by measuring the length (l) and the width (w) with calipers. Tumor volume was calculated with the formula ($V = lw^2/2$).

Immunofluorescence Staining and Immunohistochemistry. For immunofluorescence staining, cells were seeded onto coverslips and incubated overnight to establish adherence, followed by starvation in serum-free DMEM for 24 h, and then culture in complete growth medium overnight. After fixing with paraformaldehyde, cells were incubated with an antibody to β-catenin (20.0 μg/ml) at 4°C for overnight, followed by incubation with Alexa Fluor 488 conjugated secondary antibody for 1 h at room temperature and examined by using immunofluorescence microscopy (Nikon). Images were captured with IPLab imaging software (Bio Vision Technologies).

For immunohistochemistry, tissue specimens from tumor xenografts were fixed with 10% neutral-buffered formalin, and 5 μm paraffin sections prepared. One section was stained with hematoxylin and eosin (H&E) for histologic assessment, and the other sections were immunostained after antigen retrieval with boiling 10 mM sodium citrate buffer for 20 min. The primary antibodies used were rabbit polyclonal antibody to β-catenin (1:100; Biosource) at 4°C for overnight, followed by incubation with Goat anti rabbit horseradish peroxidase-conjugated antibodies (1:500) (Bio-Rad). Mayer's hematoxylin (Sigma) was used as a counterstain. Throughout the above analyses, controls were prepared by omitting the primary antibody.

RNA Interference. The siRNA derived from an mRNA sequence (AAACAUAAUGAGGACCUACAC) of mouse β-catenin as described in ref. 50 or SMARTpool siRNA, which target mouse β-catenin, were prepared by Dharmacon Research with a nontargeting duplex as negative control. siRNA (100 nM) were transfected into GSK3$\beta^{-/-}$/Ras MEFs with lipofectamine 2000 (Invitrogen) according to Invitrogen transfection protocols for mouse embryo fibroblasts. The retrovirus-mediated shRNA for mouse β-catenin was from OpenBiosystems. The virus was generated in BOSC23 packaging line and used to infect MEFs according to manufacturer instructions. The efficiency of siRNA or shRNA knockdown was confirmed by Western blotting and immunofluorescent analysis of the cellular β-catenin protein.

Statistical Analysis. Statistical analysis was carried out using the ANOVA test (for multiple groups) and the Student t test (for two groups). Differences with P values of <0.05 were considered statistically significant.

ACKNOWLEDGMENTS. The work was supported by the Lynne Cohen Foundation Ovarian Cancer Research Award (to X.F. and G.B.M.), Department of Defense Breast Cancer Research Program Fellowship Award DAMD17-03-1-0409 (to S.L.), National Institute of Health Grants CA82716 and CA64602 (to G.B.M.), National Institute of Health Core Grant P30 CA016672 (to M. D. Anderson Cancer Center), and by Canadian Institutes of Health Research.

1. Marshall CJ (1996) *Curr Opin Cell Biol* 8:197–204.
2. Hanahan D, Weinberg RA (2000) *Cell* 100:57–70.
3. Sebastian T, Malik R, Thoma S, Sage J, Johnson PF (2005) *EMBO J* 24:3301–3312.
4. Serrano M, Lin AW, McCurrach ME, Beach D, Lowe SW (1997) *Cell* 88:593–602.
5. Braig M, Lee S, Loddenkemper C, Rudolph C, Peters AH, Schlegelberger B, Stein H, Dorken B, Jenuwein T, Schmitt CA (2005) *Nature* 436:660–665.
6. Deng Q, Li Y, Tedesco D, Liao R, Fuhrmann G, Sun P (2005) *Cancer Res* 65:8298–8307.
7. Wohlgemuth S, Kiel C, Kramer A, Serrano L, Wittinghofer F, Herrmann C (2005) *J Mol Biol* 348:741–758.
8. Rowland BD, Peeper DS (2006) *Nat Rev Cancer* 6:11–23.
9. Peeper DS, Dannenberg JH, Douma S, te Riele H, Bernards R (2001) *Nat Cell Biol* 3:198–203.
10. Langley E, Pearson M, Faretta M, Bauer UM, Frye RA, Minucci S, Pelicci PG, Kouzarides T (2002) *EMBO J* 21:2383–2396.
11. Shvarts A, Brummelkamp TR, Scheeren F, Koh E, Daley GQ, Spits H, Bernards RA (2002) *Genes Dev* 16:681–686.
12. Ruiz S, Santos M, Paramio JM (2006) *Cell Cycle* 5:625–629.
13. Garcia-Tunon I, Ricote M, Ruiz A, Fraile B, Paniagua R, Royuela M (2006) *Cancer Invest* 24:119–125.
14. Adhikary S, Eilers M (2005) *Nat Rev Mol Cell Biol* 6:635–645.
15. Turnell AS, Mymryk JS (2006) *Br J Cancer* 95:555–560.
16. Kortlever RM, Higgins PJ, Bernards R (2006) *Nat Cell Biol* 8:877–884.
17. Chen Z, Trotman LC, Shaffer D, Lin HK, Dotan ZA, Niki M, Koutcher JA, Scher HI, Ludwig T, Gerald W, *et al*. (2005) *Nature* 436:725–730.
18. Bienz M, Clevers H (2000) *Cell* 103:311–320.
19. Damalas A, Kahan S, Shtutman M, ben-Ze'ev A, Oren M (2001) *EMBO J* 20:4912–4922.
20. Hinoi T, Yamamoto H, Kishida M, Takada S, Kishida S, Kikuchi A (2000) *J Biol Chem* 275:34399–34406.
21. Aberle H, Bauer A, Stappert J, Kispert A, Kemler R (1997) *EMBO J* 16:3797–3804.
22. Liu C, Kato Y, Zhang Z, Do VM, Yankner BA, He X (1999) *Proc Natl Acad Sci USA* 96:6273–6278.
23. Morin PJ, Sparks AB, Korinek V, Barker N Clevers H, Vogelstein B, Kinzler KW (1997) *Science* 275:1787–1790.
24. Rubinfeld B, Robbins P, El-Gamil M, Albert I, Porfiri E, Polakis P (1997) *Science* 275:1790–1792.
25. Woodgett JR (2001) *Sci STKE* 2001:RE12.
26. Hoeflich KP, Luo J, Rubie EA, Tsao MS, Jin O, Woodgett JR (2000) *Nature* 406:86–90.
27. Dimri GP, Lee X, Basile G, Acosta M, Scott G, Roskelley C, Medrano EE, Linskens M, Rubelj I, Pereira-Smith O, *et al.* (1995) *Proc Natl Acad Sci USA* 92:9363–9367.
28. Fang X, Yu S, LaPushin R, Lu Y, Furui T, Penn LZ, Stokoe D, Erickson JR, Bast RCJ, Mills GB (2000) *Biochem J* 352:135–143.
29. Stahle M, Veit C, Bachfischer U, Schierling K, Skripczynski B, Hall A, Gierschik P, Giehl K (2003) *J Cell Sci* 116:3835–3846.
30. Sengupta S, Kim KS, Berk MP, Oates R, Escobar P, Belinson J, Li W, Lindner DJ, Williams B, Xu Y (2007) *Oncogene* 6:2894–2901.
31. Lionel Larue L, Bellacosa A (2005) *Oncogene* 24:7443–7454.
32. Zhou BP. Deng J, Xia W, Xu J, Li YM, Gunduz M, Hung MC (2004) *Nat Cell Biol* 6:931–940.
33. Olmeda D, Jorda M, Peinado H Fabra A, Cano A (2007) *Oncogene* 26:1862–1874.
34. Ali A, Hoeflich KP, Woodgett JR (2001) *Chem Rev* 101:2527–2540.
35. MacAulay K, Doble BW, Patel S, Hansotia T, Sinclair EM, Drucker DJ, Nagy A, Woodgett JR (2007) *Cell Metab* 6:329–337.
36. Liu S, Yu S, Hasegawa Y, LaPushin R, Xu HJ, Woodgett JR, Mills GB, Fang X (2004) *J Biol Chem* 279:51075–51081.
37. Cohen P, Frame S (2001) *Nat Rev Mol Cell Biol* 2:769–776.
38. Hughes K, Nikolakaki E, Plyte SE, Totty NF, Woodgett JR (1993) *EMBO J* 12:803–808.
39. Zhang Y, Qiu WJ, Liu DX, Neo SY, He X, Lin SC (2001) *J Biol Chem* 276:32152–32159.
40. Abbosh PH, Nephew KP (2005) *Thyroid* 15:551–561.
41. Harada N, Oshima H, Katoh M, Tamai Y, Oshima M, Taketo MM (2004) *Cancer Res* 64:48–54.
42. Yost C, Torres M, Miller JR, Hung E, Kimelman D, Moon RT (1996) *Genes Dev* 10:1443–1454.
43. Uematsu K, He B, You L, Xu Z, McCormick F, Jablons DM (2003) *Oncogene* 22:7218–7221.
44. Uematsu K, Kanazama S, You L, He B, Xu Z, Li K, Peterlin BM, McCormick F, Jablons DM (2003) *Cancer Res* 63:4547–4551.
45. Yau TO, Chan CY, Chan KL, Lee MF, Wong CM, Fan ST, Ng IO (2005) *Oncogene* 24:1607–1614.
46. Gonzalez-Sancho JM, Brennan KR, Castelo-Soccio LA, Brown AM (2004) *Mol Cell Biol* 24:4757–4768.
47. Tetsu O, McCormick F (1999) *Nature* 398:422–426.
48. Shtutman M, Zhurinsky J, Simcha I, Albanese C, D'Amico M, Pestell R, Ben-Ze'ev A (1999) *Proc Natl Acad Sci USA* 96:5522–5527.
49. Diehl JA, Cheng M, Roussel MF, Sherr CJ (1998) *Genes Dev* 12:3499–3511.
50. Cong F, Schweizer L, Chamorro M, Varmus H (2003) *Mol Cell Biol* 23:8462–8470.